Heterogeneous Reactivity of Nitric Acid with Nascent Sea Spray Aerosol: Large Differences Observed between and within Individual Particles

ARTICLE *in* JOURNAL OF PHYSICAL CHEMISTRY LETTERS · AUGUST 2014

Impact Factor: 7.46 · DOI: 10.1021/jz5008802

10 AUTHORS, INCLUDING:

O. S. Ryder
University of California, San Diego
17 PUBLICATIONS **203** CITATIONS
SEE PROFILE

Jonathan V. Trueblood
University of Iowa
3 PUBLICATIONS **17** CITATIONS
SEE PROFILE

Douglas B Collins
University of California, San Diego
17 PUBLICATIONS **157** CITATIONS
SEE PROFILE

Kim Prather
University of California, San Diego
296 PUBLICATIONS **9,844** CITATIONS
SEE PROFILE

THE JOURNAL OF PHYSICAL CHEMISTRY Letters

Letter

pubs.acs.org/JPCL

Heterogeneous Reactivity of Nitric Acid with Nascent Sea Spray Aerosol: Large Differences Observed between and within Individual Particles

Andrew P. Ault,[†,#] Timothy L. Guasco,[‡,⊥] Jonas Baltrusaitis,[†,∥] Olivia S. Ryder,[‡] Jonathan V. Trueblood,[†] Douglas B. Collins,[‡] Matthew J. Ruppel,[‡] Luis A. Cuadra-Rodriguez,[‡] Kimberly A. Prather,*[,‡,§] and Vicki H. Grassian*[,†]

[†]Department of Chemistry, University of Iowa, Iowa City, Iowa 52242, United States

[‡]Department of Chemistry and Biochemistry, University of California, San Diego, La Jolla, California 92037, United States

[§]Scripps Institution of Oceanography, University of California, San Diego, La Jolla, California 92093, United States

Supporting Information

ABSTRACT: Current climate and atmospheric chemistry models assume that all sea spray particles react as if they are pure NaCl. However, recent studies of sea spray aerosol particles have shown that distinct particle types exist (including sea salt, organic carbon, and biological particles) as well as mixtures of these and, within each particle type, there is a range of single-particle chemical compositions. Because of these differences, individual particles should display a range of reactivities with trace atmospheric gases. Herein, to address this, we study the composition of individual sea spray aerosol particles after heterogeneous reaction with nitric acid. As expected, a replacement reaction of chloride with nitrate is observed; however, there is a large range of reactivities spanning from no reaction to complete reaction between and within individual sea spray aerosol particles. These data clearly support the need for laboratory studies of individual, environmentally relevant particles to improve our fundamental understanding as to the properties that determine reactivity.

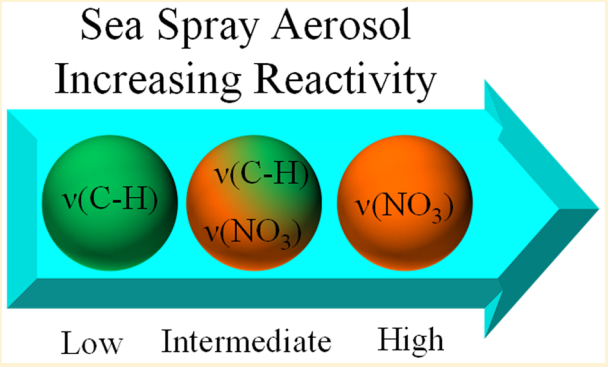

SECTION: Environmental and Atmospheric Chemistry, Aerosol Processes, Geochemistry, and Astrochemistry

Developing a better understanding of the factors controlling heterogeneous chemical reactions on the surface of atmospheric aerosols is challenging because the complex composition, structure, and heterogeneous distribution of species make predicting the degree of reactivity of each particle difficult.[1−4] As a result, simplified model systems used in laboratory studies that have provided a great deal of kinetic data[3,5−7] do not properly emulate the complexity of atmospheric aerosols and thus cannot fully account for chemical processes occurring in the real world.[1,7−12] Sea spray aerosol (SSA) particles, in particular, represent an abundant source of particulate matter in air,[13] yet the size-dependent chemical composition of individual nascent SSA particles has been difficult to determine in the environment for several reasons,[14] including the presence and interference from background aerosols.[1] Recently, as discussed in Prather et al.,[1] the size-resolved chemical composition and mixing state distribution of SSA particles have been measured from breaking waves for the first time with minimal influence from background aerosol, using a unique ocean-atmosphere facility (Figure 1). The SSA particle number size distribution peaks at ∼162 nm (Figure 2).[1,15,16] However, when considering heterogeneous reactions that require gas-phase collisions at the particle surface, the surface area per unit air volume (e.g., $\mu m^2/m^3$) is a key metric for evaluating the critical sizes for heterogeneous reactions in the atmosphere.[7,10] This distribution when plotted in terms of surface area can be calculated according to eq E1

$$\frac{dS}{d\log D_p} = \frac{dN}{d\log D_p} \times \pi(D_p)^2 \quad \text{(E1)}$$

where the $dS/d\log D_p$ is the log-normal surface area concentration, D_p is the geometric diameter, and $dN/d\log D_p$ is the log-normal number concentration. The surface area distribution peaks with a mean diameter at 1.2 μm and ranges from ∼0.5 to 2.5 μm. Most methods for studying heterogeneous chemistry reactions are based on evaluating ensemble averages.[7] However, the presence of an organic layer on the surface of a SSA particle can inhibit the uptake of

Received: May 4, 2014
Accepted: July 2, 2014
Published: July 2, 2014

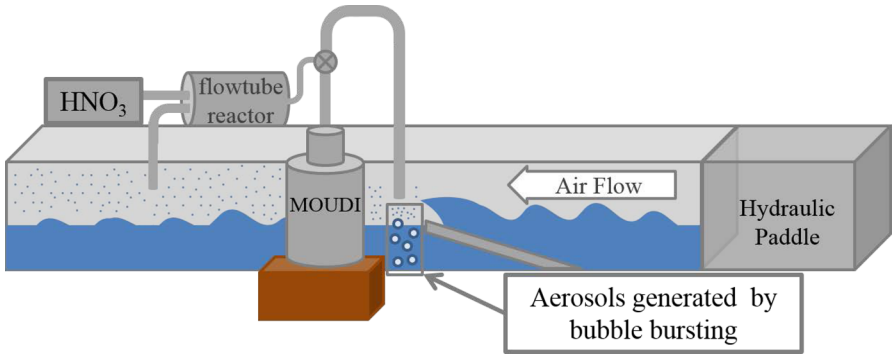

Figure 1. Simplified schematic diagram of the experimental setup of a wave flume at the Scripps Institution of Oceanography Hydraulics Laboratory. The multiorifice uniform deposition impactor (MOUDI) and flow tube reactor are also shown.

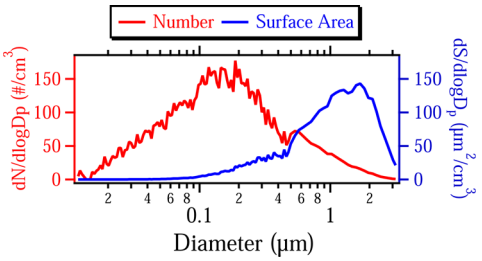

Figure 2. Number and surface area size distributions of SSA particles produced at the wave flume.

reactive nitrogen species (i.e., HNO_3 or N_2O_5),[3] which has important implications for global NO_x budgets.[17] This organic layer can have varying composition and thickness between different SSA particles.[2,18−20] Understanding how different organic layer properties can impact reactivity is crucial. Bulk ensemble measurements provide valuable information, but the implicit assumption of internal mixing can lead to discrepancies between models and measurements because the average value may not accurately represent the aerosol population when multiple populations are present. As an example of the importance of mixing state, Ryder et al. showed that parametrizations of $\gamma(N_2O_5)$ were roughly equal to measurements under clean conditions, but internal mixing led to an overestimation of $\gamma(N_2O_5)$ by a factor of 3 for conditions where organic matter can form an organic film or impact particle water concentrations.[21] Thus, to accurately describe the heterogeneous chemistry of reactive nitrogen oxide gases on SSA, it is important to evaluate individual particle-to-particle variability. In addition, recent fundamental measurements of the distribution of species within individual particles via optical tweezers have shown that particles not only exist as homogeneous and core−shell morphologies, but also as partially engulfed, amorphous microphysical states.[22]

To probe the reactivity of different particles, it is critical to establish the contributions of specific types to the overall population of particles in the key size range identified in Figure 2. Table 1 shows the fractional abundance of particle types identified in nascent SSA previously,[1] but specifically in the size range where surface area dominates. The key types in order of fractional abundance are sea salt mixed with organic carbon (SS−OC), sea salt particles (SS), biological (Bio), and organic carbon particles (OC).[1] SS is defined as primarily inorganic salts, SS−OC is a mix of inorganic salts and OC, Bio particles show markers of biological origin (from mass spec signatures) and can be associated with metals,[23] and OC is organic

Table 1. Particle Types in SSA in the Surface Area Mode (0.5 to 2.5 μm)

	type				
	sea salt (SS)	organic carbon (OC)	sea salt with organic carbon (SS−OC)	biological (Bio)	contamination
number fraction	0.41	0.02	0.46	0.08	0.03

carbon.[1,18] Number fractions were calculated by taking the fraction of each type in each size bin (between 0.5 and 2.5 μm) and multiplying by the relative contribution of that bin to the overall size distribution (0.5−2.5 μm). Uncertainty in these values results from the number of particles analyzed per bin, which contained hundreds of particles. SS−OC plus SS represented greater than ca. 86% of particles between 0.5 and 2.5 μm.[18]

In order to probe the physicochemical changes of the freshly generated SSA after heterogeneous reaction with reactive nitrogen species of atmospheric importance (in this case, nitric acid),[7] a flow tube reactor was attached to the wave flume[1] or marine aerosol reference tank (MART, a portable system that generates the SSA similar to the wave flume),[24] where particles were exposed to nitric acid (Figure 1) and then analyzed.[2] To determine the extent of changes in surface composition due to heterogeneous reactions, high-resolution XPS data recorded in the Cl 2p (Figure 3a) and N 1s (Figure 3b) regions for unreacted and reacted particles deposited onto a silicon substrate from ∼1−2 μm were compared. For the unreacted particles, the doublet in the Cl 2p region[25,26] indicates that after dehydration/efflorescence in the vacuum chamber, chloride is present at the particle interface. No peak for Cl 2p was observed for the reacted particles, which indicates that the small amount of Cl remaining is below the detection limit (and in a low percentage of particles, as shown below) or not present at the particle surface. High-resolution spectra in the N 1s region show that for unreacted particles, there is no nitrate present, as indicated by the absence of a peak with a binding energy of ∼407 eV. For reacted particles, a distinct peak at 407 eV for nitrate is observed (Figure 3).[27] More specifically, nitrogen is in the +5 oxidation state, which means that the nitrogen is in the form of the nitrate anion. With these ensemble average data, these experiments would appear to follow the heterogeneous reaction of the sodium chloride component of SSA particles with nitric acid according to reaction R1.[28−30] However, SSA has many other components not accounted for in this reaction (cations: Mg^{2+}, K^+, Ca^{2+}; anions: SO_4^{2-}; and organics species:

dx.doi.org/10.1021/jz5008802 | J. Phys. Chem. Lett. 2014, 5, 2493−2500

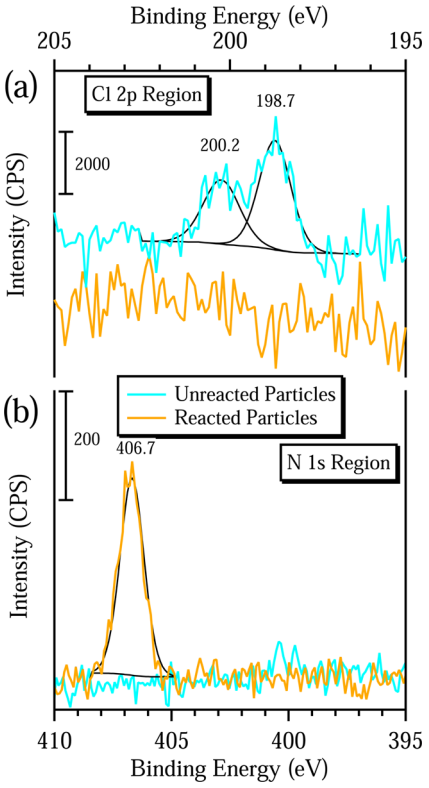

Figure 3. (a) High-resolution XPS data in the Cl 2p binding region and (b) the N 1s binding region for unreacted particles and reacted particles. The unreacted particles show the Cl $2p_{3/2}$ (198.7) and $2p_{1/2}$ (200.2 eV) peaks, and the reacted particle clearly shows a peak associated with nitrate at 406.7 ± 0.2 eV. These peaks have been fit with a Gaussian-Lorentzian lineshape.

long-chain aliphatic species, lipopolysaccharides, etc.) that can lead to differing behavior between subpopulations of particles after heterogeneous reactions, including cation redistribution and changes to the organic layer.[2]

$$HNO_{3(g)} + NaCl_{(aq)} \rightarrow NaNO_{3(aq)} + HCl_{(g)} \quad (R1)$$

Given the particle loading on the substrate and size of the X-ray beam (700 × 300 μm),[31] it is estimated that ~1 × 10^4 particles were analyzed in a given spectrum. Something that is not addressed in these measurements is that the compositions of different types of particles are averaged together and thus cannot be used to assess any particle-to-particle variability in reactivity. Individual particle information is needed to evaluate climate-relevant properties, such as cloud condensation and ice nucleation, optical scattering/absorption, and hygroscopic growth that occur at the single-particle level; mass averages do not adequately tie the properties back to fundamental physical chemistry principles.[8]

In order to probe the degree and variability of processing by heterogeneous reactions with nitric acid in real time, aerosol time-of-flight mass spectrometry (ATOFMS) data were used to probe the size and chemical composition of single particles generated with a MART.[24,32] To evaluate the extent of chloride depletion, the chloride fraction of summed chloride + nitrate intensity ($^{35}Cl^-/(^{35}Cl^- + NO_3^-)$) is shown as a function of size in Figure 4. The $^{35}Cl^-$ and $^{62}NO_3^-$ peak areas for unreacted and reacted particles are given in Figure S1 of the Supporting Information. As seen in Figure 4, while ~90% of the particles have undergone significant chloride replacement, a number of

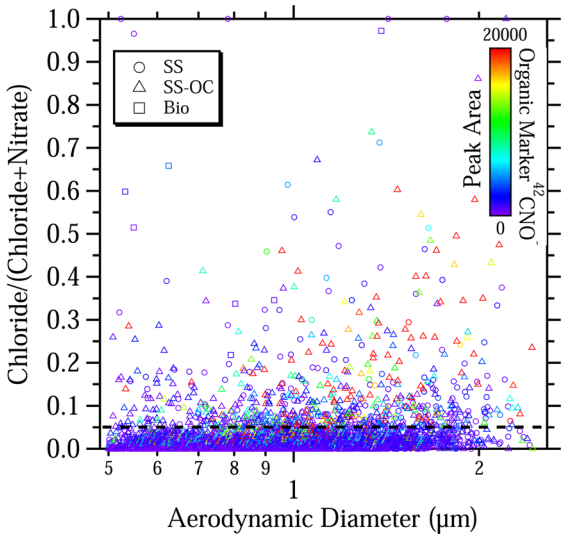

Figure 4. ATOFMS ratio of the chloride fraction to the total chloride plus nitrate signal for reacted particles as a function of aerodynamic diameter, for the different particle types: sea salt (SS); sea salt with organic carbon (SS-OC); and biological (Bio). The dashed line at 5% is used to distinguish highly reacted particles from less reacted particles. The color represents the peak area of the OC marker $^{42}CNO^-$, with red indicating higher intensity.

particles have undergone minimal reaction. To understand the controlling factors for this range of reactivities, the key chemical differences between more and less reacted particles need to be identified. The colors of the individual points in Figure 4 are related to the intensity of $^{42}CNO^-$, a peak that is indicative of organic species (likely biogenically derived).[33] These ions in SSA are predominantly associated with SS−OC and Bio particles.[1] These results indicate that biogenically derived organic species in individual SS−OC particles or Bio particles can inhibit heterogeneous reactivity of individual particles.

Figure 5 shows the difference between the averaged mass spectra for all single particles that were either highly reacted or less reacted to show which species are enhanced in the two populations of particles. For the more reacted particles, these spectra are dominated by $^{23}Na^+$, $^{62}NO_3^-$, and associated sodium nitrate clusters. For the less reacted particles, along with $^{35}Cl^-$ and NaCl clusters ($^{81,83}Na_2Cl^+$ and $^{93,95,97}NaCl_2^-$), three distinguishing features are observed, (1) organic nitrogen: $^{26}CN^-$, $^{42}CNO^-$, and $^{59}N(CH_3)_2^+$, (2) phosphate: $^{47}PO^-$, $^{63}PO_2^-$, and $^{79}PO_3^-$, and (3) metal and metal oxides: $^{40}Ca^+$ and $^{56}CaO^+/^{56}Fe^+$.[23] Some of these more distinguishing mass spectral features and differences are highlighted in Figure 5.

In order to further understand the differences in the mass spectrometry data, additional single-particle analyses were done. In particular, SSA particles collected on quartz substrates after passing through the flow tube reactor were analyzed using micro-Raman spectroscopy, a powerful method for probing the distribution of chemical species within individual particles.[34] The spatial information from imaging the distribution of chemical species within individual particles provides a way to identify features within different subpopulations of reacted particles with less chloride displacement.

Raman spectra, optical images, and spectral mapping of different functional groups, including $\nu_s(NO_3^-)$ and ν(C−H) stretching regions, are shown in Figure 6. A total of 67 Raman spectra of individual particles were collected of individual

dx.doi.org/10.1021/jz5008802 | J. Phys. Chem. Lett. 2014, 5, 2493−2500

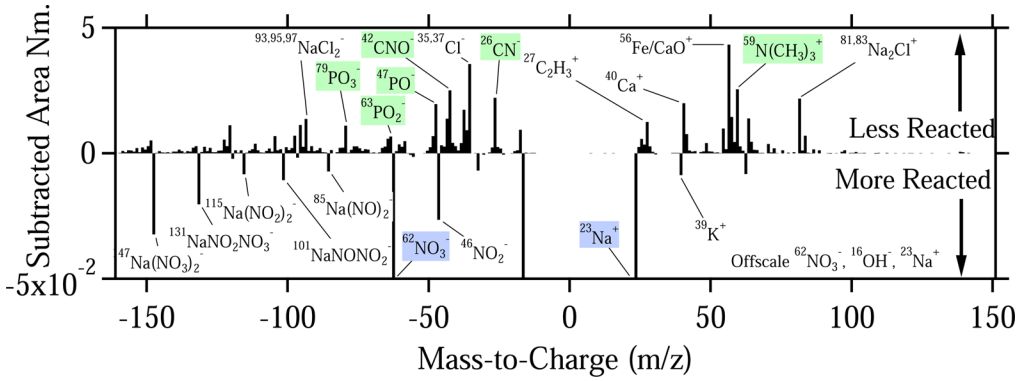

Figure 5. Mass spectral subtraction plot of normalized peak areas for average mass spectra of particles with >5% $Cl^-/(Cl^- + NO_3)$ (positive values) versus less than 5% $Cl/(Cl^- + NO_3^-)$ (negative values). Several distinguishing features are highlighted in these average mass spectra.

particles, and representative spectra are grouped according to three different particle types with respect to their reactivity. In particular, particles are identified as those showing high (31 collected), low (13 collected), and intermediate reactivity (23 collected). These identifications are based on the relative intensities of peaks due to $\nu_s(NO_3^-)$ and ν(C−H) within individual particles and related to identified particle types below. For example, in Figure 6a, particle spectra are overlaid for particles that are identified as highly reactive. These particles have an intense nitrate signal due to several of the vibrational modes associated with the nitrate anion, including the very intense symmetric stretch at 1068 cm^{-1}. These particles also show minimal peak intensity in the ν(C−H) stretching region. The inset shown in Figure 6a is for the optical image of one highly reacted SS particle, a spectrum collected at a particular spot on that particle, and a spectral map of the nitrate signal by collecting Raman spectra for that single particle. This shape correlates with a cubic shape likely indicating less organic material disrupting crystallization for the $NaNO_3$.[18]

The Raman spectra for particles with minimal or low reactivity are shown in Figure 6b, and the particles are likely SS−OC or Bio. Differences in these particle spectra, beyond having little to no peak intensity in the $\nu_s(NO_3^-)$ nitrate region, include high peak intensities in the ν(C−H) stretching region and features in the δ(C−H) bending region. The optical image and chemical mapping of the organic component (as determined by the peak at 2880 cm^{-1}) are shown in the inset of Figure 6, with a less cubic structure indicative of organic material inhibiting crystallization. The mapping shows that this particle contains a large fraction of organic compounds.

For the third category of particles, those exhibiting intermediate reactivity, Raman spectra are shown in Figure 6c. For these particles, Raman spectra show intermediate intensity in both the $\nu_s(NO_3^-)$ and ν(C−H) regions. Interestingly, for these particles of intermediate reactivity, the nitrate-rich and organic-rich regions are seen segregated and not co-located, as shown by the spectral maps in the inset in Figure 6c. Thus, these spectral maps suggest that not only is there variability of reactivity between different particles, but, in fact, these reactions may be spatially inhomogeneous within individual SSA particles, particularly SS−OC with aqueous and organic phases.[2] These particles with intermediate reactivity have some variability in the amount and type of organic species, as shown in the fingerprint and C−H stretching region for additional spectra provided in the Supporting Information.[19] Furthermore, the Raman maps shown in Figure 6c qualitatively differ from the uniform concentrated organic coating observed with electron microscopy techniques under vacuum conditions.[2] These differences are currently the focus of future investigations.

One other interesting observation from the single-particle micro-Raman data for these reacted particles is that shifts in the frequency $\nu_s(NO_3^-)$ mode depend on the water content of the particle. Particles were generated in a liquid state and reacted at 60% relative humidity (RH) (no efflorescence) before collection and subsequent drying on the substrates prior to and during storage. Many particles examined under the relatively dry, low RH conditions of this study show a nitrate frequency of 1068 cm^{-1}, whereas a few particles exhibit a nitrate peak at a lower frequency closer to 1055 cm^{-1} when the nitrate ion is in an aqueous environment.[35] These particles that exhibit lower-frequency $\nu_s(NO_3^-)$ modes also show a broad peak in the O−H stretching region near 3400 cm^{-1} indicative of water associated with the particle. Figure 7a shows 20 spectra with peaks at 1068 cm^{-1}, the $\nu_s(NO_3^-)$ for $NaNO_3$, and two spectra with peaks at 1055 cm^{-1}, which is the peak for the nitrate anion in aqueous solution. Only the two spectra associated with the nitrate anion with a frequency of 1055 cm^{-1} have intensity in the O−H stretching region (Figure 7b), indicating a correlation between the nitrate anion environment and the presence of O−H stretching. This aqueous nitrate is likely due to either encapsulation of water in a thin organic layer or the formation of a glassy state that can retain water.[36] The Raman spectral maps and an optical image for a particle that contains water, as evidenced by the presence of an O−H stretching band, and the nitrate band at 1055 cm^{-1} are shown in Figure 7c. The overlap of the spectral maps and image further highlight the coexistence of these two components (water and nitrate ion) in the particle. These results demonstrate the utility of ambient pressure micro-Raman spectroscopy of aerosol particles to determine the physical state and spatial distribution of species within the particle and different states of hydration for individual particles that are heterogeneous in their nature, such as SSA particles.

In summary, this study provides several interesting results and conclusions that can be derived from the analysis of the reactivity of individual, atmospherically relevant SSA particles using single-particle methods. First, it is clearly shown that there is a range of reactivities observed (from 100% chloride displacement to <1%, Figure 4), which contrasts most atmospheric chemistry and climate models that must assume a single reactive uptake coefficient for SSA.[7] Under the conditions of this MART reactivity experiment, most particles

dx.doi.org/10.1021/jz5008802 | J. Phys. Chem. Lett. 2014, 5, 2493−2500

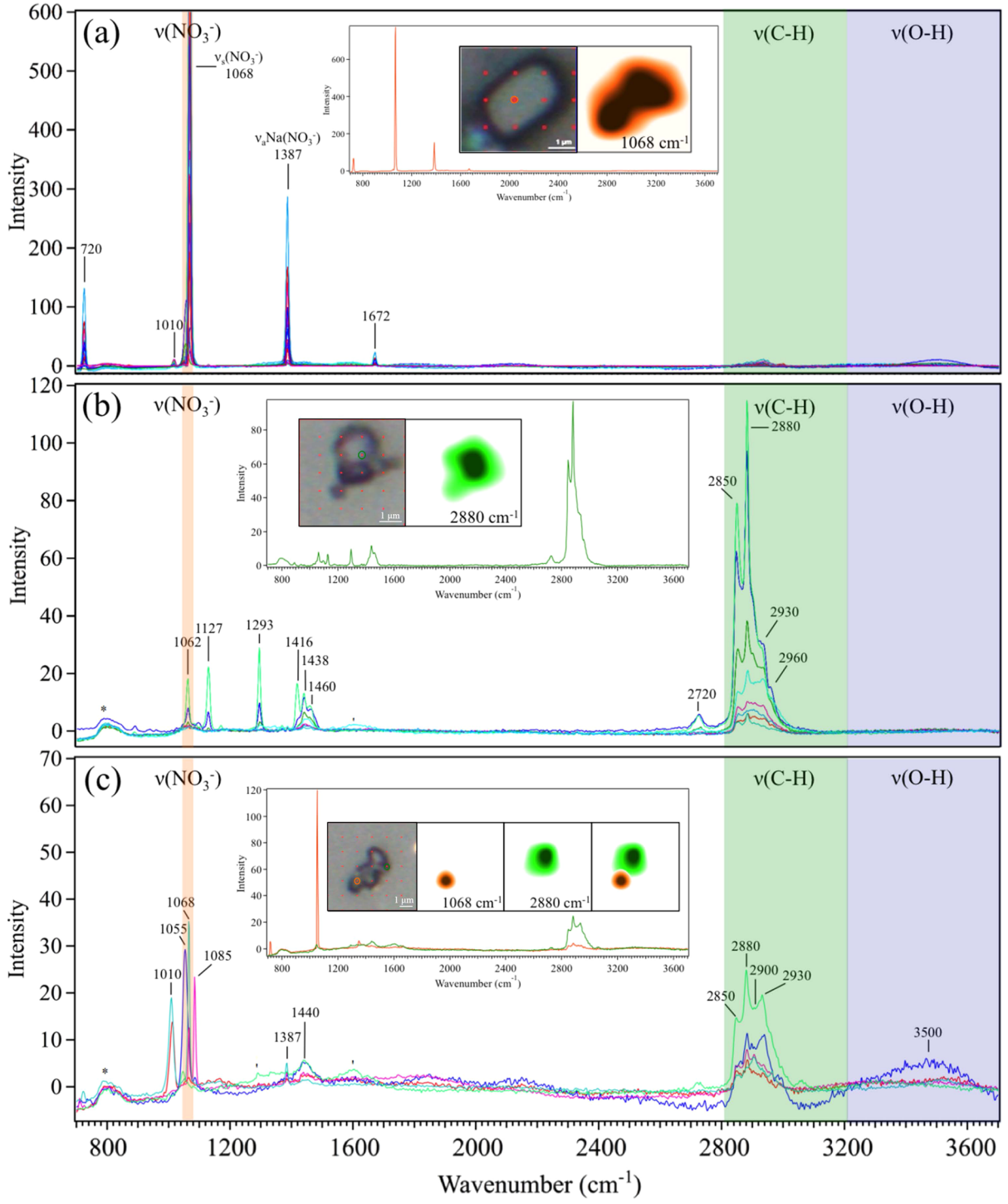

Figure 6. Raman spectra of individual SSA particles analyzed with micro-Raman spectroscopy for several different particle types, along with optical images, individual spectra, and spectral maps in the insets. The larger colored circles on the optical images indicate the locations of the particle that the laser beam interrogates for each of the spectra shown in the inset. The smaller dots represent the grid that defines the points used for the spectral maps. These spectra of particles exposed to nitric acid show different particle types. (a) Particles with high reactivity as indicated by an intense signal for the symmetric stretch of the nitrate ion at 1068 cm^{-1}, along with other nitrate vibrations. These particles also show minimal intensity in the C−H stretching region, indicating small amounts of organic species present within these particles. (b) Particles with high intensity due to organic species, as shown by the large intensity in the C−H stretching region indicating high levels of organics associated with the particle but minimal signal associated with the nitrate ion. These particles have low reactivity. (Note: Although there is a peak at 1062 cm^{-1} close to the NO_3^- region, it is most likely due to vibrations associated with the organic species within these particles, e.g., C−C stretches, C−O stretches, and/or methyl deformations, associated with the organic species present as its intensity correlates with other peaks due to organics from 1100 to 1500 cm^{-1}.) (c) Particles with both peaks associated with organic species and a nitrate anion, indicating particles with intermediate reactivity. Spectral maps are shown for the $\nu_s(NO_3^-)$ mode (1068 cm^{-1}) and ν(C−H) mode at 2880 cm^{-1}. For these particles, spectral maps along with the optical image show phase segregation between the nitrate and organic species within the particle. * designates the quartz substrate, and ' designates a small amount of graphitic carbon from sample damage by the laser.

dx.doi.org/10.1021/jz5008802 | J. Phys. Chem. Lett. 2014, 5, 2493−2500

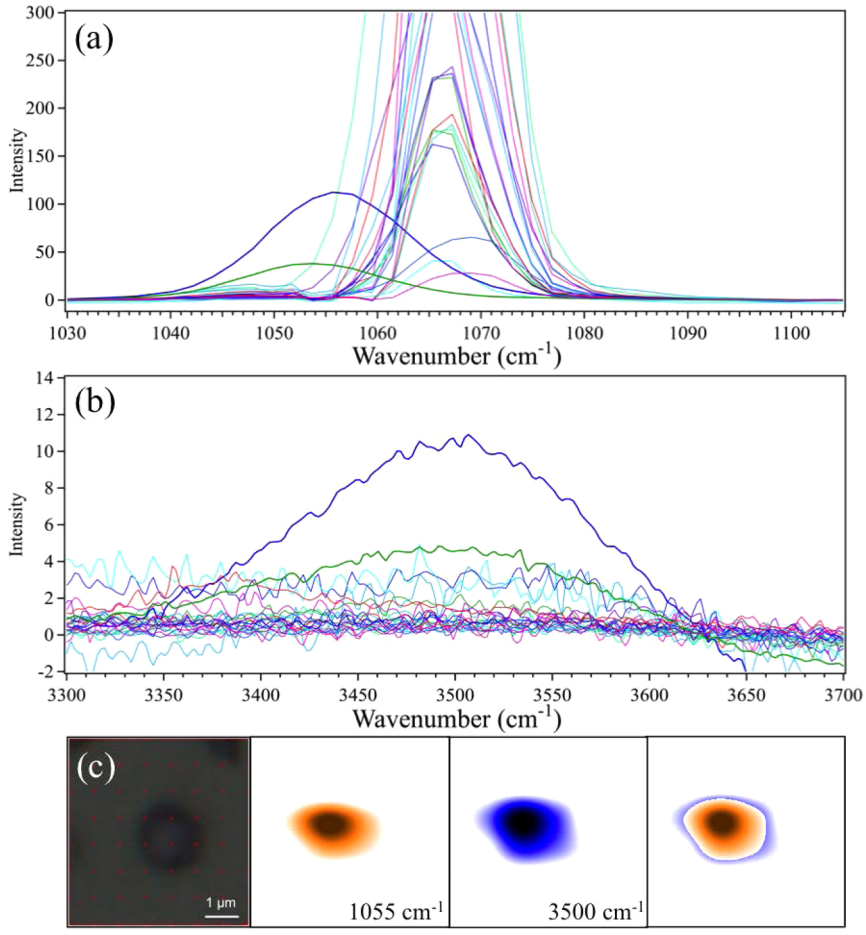

Figure 7. Raman spectra of SSA particles reacted with nitric acid in the $\nu_s(NO_3^-)$ and ν(O−H) regions. (a) Some reacted particles show different values of the frequency for the $\nu_s(NO_3^-)$ mode (1055 cm^{-1}) but do not show corresponding organic peaks that would indicate that it was a peak associated with organic species within the particle. Instead, these differences are associated with the nitrate ion in different phases, solid versus aqueous.[36] (b) Raman measurements in the spectral region associated with the O−H stretching region (~3500 cm^{-1}) indicate the presence of water associated with particles that exhibit nitrate ion peaks with lower frequency of 1055 cm^{-1}. (c) Optical image and spectral maps of $\nu_s(NO_3^-)$ and ν(O−H) stretching regions (greater orange or blue represents greater intensity of that peak), as well as their overlap, indicating co-location within the particle.

are highly reacted (only 10% of particles have >5% of chloride remaining). However, SS−OC particles (14% not reacted, 484 out of 3445 particles) are twice as likely to not undergo extensive reaction compared to those identified as SS (7%, 228 out of 3479). Although Bio type particles are primarily >1 μm (similar to SS particles), a much higher fraction retained chloride (41%, 14 out of 34 particles), although it is important to note that there were far fewer particles. Taken together, these data, along with other recent studies,[21] show that composition is a critical determinant in reactivity of SSA. These data also shine light on the fact that the approach of using a single rate constant to model chloride displacement, such as the nitric acid reaction with NaCl in reaction R1, for all SSAs is a gross oversimplification. Second, and of particular interest, is the inhibition of reactivity by organic matter of biological origin, primarily in SS−OC. Third, the evidence that particle reactivity may be spatially heterogeneous within particles builds upon recent studies by Reid and co-workers that show that organic material can be distributed asymmetrically for suspended particles,[22,37,38] though at least some particles have a radial distribution.[2] Further studies of heterogeneous reactivity of individual SSA particles are warranted in order to understand how reactions proceed on populations of particles with differing levels of chloride displacement. In addition, the spatial heterogeneity of species within particles may lead to different portions of a particle reacting with different rates of reaction, which needs to be explored. It is clear that the use of single-particle methods is needed to further understand the physical chemistry of heterogeneous reactions in the atmosphere.

■ EXPERIMENTAL SECTION

Measurements were made of nascent SSAs collected using a sealed ocean-atmosphere facility with actual breaking waves at the Scripps Institution of Oceanography (SIO) Hydraulics Laboratory, which has been determined to produce SSA with the same size and composition as the ocean.[1,18] Further details on the experimental setup are given in the Supporting Information. SSA particles were collected on substrates (quartz and silicon wafers) using a multiorifice uniform deposition impactor (MOUDI). During heterogeneous reactivity experiments, entrained aerosols from the wave channel[1] or MART[24] flowed through a custom-built, moveable-injector aerosol flow reactor that has been described in detail previously.[21] The MART was used for further studies after intensive measurements at the wave flume were completed and the flume was no

dx.doi.org/10.1021/jz5008802 | J. Phys. Chem. Lett. 2014, 5, 2493−2500

longer available (specifically the ATOFMS results). As Stokes et al.[24] show, the size distributions of SSA particles from MART are nearly identical to those from the wave flume apparatus. The SSAs generated for both methods are liquid in nature under the conditions in which they were generated and reacted with HNO_3. Offline analysis of the unreacted and reacted particles was conducted using micro-Raman spectroscopy and X-ray photoelectron spectroscopy (XPS). ATOFMS was used to measure the size and chemical composition of individual particles in real time. Methods are described further in the Supporting Information.

■ ASSOCIATED CONTENT

Supporting Information

Description of the sea spray aerosol particle generation, the aerosol flow reactor, off-line analysis of substrate-deposited particles, on-line analysis of aerosol, and additional micro-Raman spectroscopy data of single particles. This material is available free of charge via the Internet at http://pubs.acs.org.

■ AUTHOR INFORMATION

Corresponding Authors

*E-mail: kprather@ucsd.edu (K.A.P.).
*E-mail: vicki-grassian@uiowa.edu (V.H.G.).

Present Addresses

[#]A.P.A.: Department of Environmental Health Sciences and Department of Chemistry, University of Michigan, Ann Arbor, MI, 48109.
[⊥]T.L.G.: Department of Chemistry, Millikin University, Decatur, IL, 62522.
[∥]J.B.: Department of Chemical and Biomolecular Engineering Lehigh University, Bethlehem, PA 18015.

Notes

The authors declare no competing financial interest.

■ ACKNOWLEDGMENTS

The authors thank all collaborators involved with the CAICE intensive campaign and the SIO Hydraulics Laboratory staff. This work was funded by the National Science Foundation through the Center for Chemical Innovation program under Grant CHE1305427.

■ REFERENCES

(1) Prather, K. A.; Bertram, T. H.; Grassian, V. H.; Deane, G. B.; Stokes, M. D.; DeMott, P. J.; Aluwihare, L. I.; Palenik, B. P.; Azam, F.; Seinfeld, J. H.; et al. Bringing the Ocean into the Laboratory to Probe the Chemical Complexity of Sea Spray Aerosol. *Proc. Natl. Acad. Sci. U.S.A.* **2013**, *110*, 7550−7555.

(2) Ault, A. P.; Guasco, T. L.; Ryder, O. S.; Baltrusaitis, J.; Cuadra-Rodriguez, L. A.; Collins, D. B.; Ruppel, M. J.; Bertram, T. H.; Prather, K. A.; Grassian, V. H. Inside versus Outside: Ion Redistribution in Nitric Acid Reacted Sea Spray Aerosol Particles as Determined by Single Particle Analysis. *J. Am. Chem. Soc.* **2013**, *135*, 14528−14531.

(3) McNeill, V. F.; Patterson, J.; Wolfe, G. M.; Thornton, J. A. The Effect of Varying Levels of Surfactant on the Reactive Uptake of N_2O_5 to Aqueous Aerosol. *Atmos. Chem. Phys.* **2006**, *6*, 1635−1644.

(4) You, Y.; Smith, M. L.; Song, M.; Martin, S. T.; Bertram, A. K. Liquid−Liquid Phase Separation in Atmospherically Relevant Particles Consisting of Organic Species and Inorganic Salts. *Int. Rev. Phys. Chem.* **2014**, *33*, 43−77.

(5) Cosman, L. M.; Knopf, D. A.; Bertram, A. K. N_2O_5 Reactive Uptake on Aqueous Sulfuric Acid Solutions Coated with Branched and Straight-Chain Insoluble Organic Surfactants. *J. Phys. Chem. A* **2008**, *112*, 2386−2396.

(6) Knopf, D. A.; Cosman, L. M.; Mousavi, P.; Mokamati, S.; Bertram, A. K. A Novel Flow Reactor for Studying Reactions on Liquid Surfaces Coated by Organic Monolayers: Methods, Validation, and Initial Results. *J. Phys. Chem. A* **2007**, *111*, 11021−11032.

(7) Abbatt, J. P. D.; Lee, A. K. Y.; Thornton, J. A. Quantifying Trace Gas Uptake to Tropospheric Aerosol: Recent Advances and Remaining Challenges. *Chem. Soc. Rev.* **2012**, *41*, 6555−6581.

(8) Prather, K. A.; Hatch, C. D.; Grassian, V. H. Analysis of Atmospheric Aerosols. *Annu. Rev. Anal. Chem.* **2008**, *1*, 485−514.

(9) Laskin, J.; Laskin, A.; Nizkorodov, S. A. New Mass Spectrometry Techniques for Studying Physical Chemistry of Atmospheric Heterogeneous Processes. *Int. Rev. Phys. Chem.* **2013**, *32*, 128−170.

(10) Kolb, C. E.; Cox, R. A.; Abbatt, J. P. D.; Ammann, M.; Davis, E. J.; Donaldson, D. J.; Garrett, B. C.; George, C.; Griffiths, P. T.; Hanson, D. R.; et al. An Overview of Current Issues in the Uptake of Atmospheric Trace Gases by Aerosols and Clouds. *Atmos. Chem. Phys.* **2010**, *10*, 10561−10605.

(11) Bertram, T. H.; Thornton, J. A.; Riedel, T. P.; Middlebrook, A. M.; Bahreini, R.; Bates, T. S.; Quinn, P. K.; Coffman, D. J. Direct Observations of N_2O_5 Reactivity on Ambient Aerosol Particles. *Geophys. Res. Lett.* **2009**, *36*, L19803 DOI: 10.1029/2009GL040248.

(12) You, Y.; Renbaum-Wolff, L.; Carreras-Sospedra, M.; Hanna, S. J.; Hiranuma, N.; Kamal, S.; Smith, M. L.; Zhang, X.; Weber, R. J.; Shilling, J. E.; Dabdub, D.; Martin, S. T.; Bertram, A. K. Images Reveal that Atmospheric Particles Can Undergo Liquid−Liquid Phase Separations. *Proc. Natl. Acad. Sci. U.S.A.* **2012**, *109*, 13188−13193.

(13) Andreae, M. O.; Rosenfeld, D. Aerosol-Cloud-Precipitation Interactions. Part 1. The Nature and Sources of Cloud-Active Aerosols. *Earth-Sci. Rev.* **2008**, *89*, 13−41.

(14) Donaldson, D. J.; George, C. Sea-Surface Chemistry and Its Impact on the Marine Boundary Layer. *Environ. Sci. Technol.* **2012**, *46*, 10385−10389.

(15) de Leeuw, G.; Andreas, E. L.; Anguelova, M. D.; Fairall, C. W.; Lewis, E. R.; O'Dowd, C.; Schulz, M.; Schwartz, S. E. Production Flux of Sea Spray Aerosol. *Rev. Geophys.* **2011**, *49*, rg000349 DOI: 10.1029/2010RG000349.

(16) Lewis, R.; Schwartz, E. *Sea Salt Aerosol Production: Mechanisms, Methods, Measurements and Models — A Critical Review*; AGU: Washington, DC, 2004.

(17) Evans, M. J.; Jacob, D. J. Impact of New Laboratory Studies of N_2O_5 Hydrolysis on Global Model Budgets of Tropospheric Nitrogen Oxides, Ozone, and OH. *Geophys. Res. Lett.* **2005**, *32*, L09813 DOI: 10.1029/2005GL022469.

(18) Ault, A. P.; Moffet, R. C.; Baltrusaitis, J.; Collins, D. B.; Ruppel, M. J.; Cuadra-Rodriguez, L. A.; Zhao, D.; Guasco, T. L.; Ebben, C. J.; Geiger, F. M.; et al. Size-Dependent Changes in Sea Spray Aerosol Composition and Properties with Different Seawater Conditions. *Environ. Sci. Technol.* **2013**, *47*, 5603−5612.

(19) Ault, A. P.; Zhao, D.; Ebben, C. J.; Tauber, M. J.; Geiger, F. M.; Prather, K. A.; Grassian, V. H. Raman Microspectroscopy and Vibrational Sum Frequency Generation Spectroscopy as Probes of the Bulk and Surface Compositions of Size-Resolved Sea Spray Aerosol Particles. *Phys. Chem. Chem. Phys.* **2013**, *15*, 6206−6214.

(20) Ebben, C. J.; Ault, A. P.; Ruppel, M. J.; Ryder, O. S.; Bertram, T. H.; Grassian, V. H.; Prather, K. A.; Geiger, F. M. Size-Resolved Sea Spray Aerosol Particles Studied by Vibrational Sum Frequency Generation. *J. Phys. Chem. A* **2013**, *117*, 6589−6601.

(21) Ryder, O. S.; Ault, A. P.; Cahill, J. F.; Guasco, T. L.; Riedel, T. P.; Cuadra-Rodriguez, L. A.; Gaston, C. J.; Fitzgerald, E.; Lee, C.; Prather, K. A.; Bertram, T. H. On the Role of Particle Inorganic Mixing State in the Reactive Uptake of N_2O_5 to Ambient Aerosol Particles. *Environ. Sci. Technol.* **2014**, *48*, 1618−1627.

(22) Krieger, U. K.; Marcolli, C.; Reid, J. P. Exploring the Complexity of Aerosol Particle Properties and Processes Using Single Particle Techniques. *Chem. Soc. Rev.* **2012**, *41*, 6631−6662.

(23) Guasco, T. L.; Cuadra-Rodriguez, L. A.; Pedler, B. E.; Ault, A. P.; Collins, D. B.; Zhao, D.; Kim, M. J.; Ruppel, M. J.; Wilson, S. C.; Pomeroy, R. S.; et al. Transition Metal Associations with Primary

Biological Particles in Sea Spray Aerosol Generated in a Wave Channel. *Environ. Sci. Technol.* **2013**, *48*, 1324−1333.
(24) Stokes, M. D.; Deane, G. B.; Prather, K. A.; Bertram, T. H.; Ruppel, M. J.; Ryder, O. S.; Brady, J. M.; Zhao, D. A Marine Aerosol Reference Tank System as a Breaking Wave Analogue for the Production of Foam and Sea-Spray Aerosols. *Atmos. Meas. Technol.* **2013**, *6*, 1085−1094.
(25) Shchukarev, A.; Boily, J. F.; Felmy, A. R. XPS of Fast-Frozen Hematite Colloids in NaCl Aqueous Solutions: I. Evidence for the Formation of Multiple Layers of Hydrated Sodium and Chloride Ions Induced by the {001} Basal Plane. *J. Phys. Chem. C* **2007**, *111*, 18307−18316.
(26) Wren, A. G.; Phillips, R. W.; Tolentino, L. U. Surface Reactions of Chlorine Molecules and Atoms with Water and Sulfuric Acid at Low Temperatures. *J. Colloid Interface Sci.* **1979**, *70*, 544−557.
(27) Baltrusaitis, J.; Jayaweera, P. M.; Grassian, V. H. XPS Study of Nitrogen Dioxide Adsorption on Metal Oxide Particle Surfaces under Different Environmental Conditions. *Phys. Chem. Chem. Phys.* **2009**, *11*, 8295−8305.
(28) Gard, E. E.; Kleeman, M. J.; Gross, D. S.; Hughes, L. S.; Allen, J. O.; Morrical, B. D.; Fergenson, D. P.; Dienes, T.; Galli, M. E.; Johnson, R. J.; Cass, G. R.; Prather, K. A. Direct Observation of Heterogeneous Chemistry in the Atmosphere. *Science* **1998**, *279*, 1184−1187.
(29) Finlayson-Pitts, B. J.; Hemminger, J. C. Physical Chemistry of Airborne Sea Salt Particles and Their Components. *J. Phys. Chem. A* **2000**, *104*, 11463−11477.
(30) Krueger, B. J.; Grassian, V. H.; Iedema, M. J.; Cowin, J. P.; Laskin, A. Probing Heterogeneous Chemistry of Individual Atmospheric Particles Using Scanning Electron Microscopy and Energy-Dispersive X-ray Analysis. *Anal. Chem.* **2003**, *75*, 5170−5179.
(31) Baltrusaitis, J.; Chen, H.; Rubasinghege, G.; Grassian, V. H. Heterogeneous Atmospheric Chemistry of Lead Oxide Particles with Nitrogen Dioxide Increases Lead Solubility: Environmental and Health Implications. *Environ. Sci. Technol.* **2012**, *46*, 12806−12813.
(32) Pratt, K. A.; Mayer, J. E.; Holecek, J. C.; Moffet, R. C.; Sanchez, R. O.; Rebotier, T. P.; Furutani, H.; Gonin, M.; Fuhrer, K.; Su, Y. X.; Guazzotti, S.; Prather, K. A. Development and Characterization of an Aircraft Aerosol Time-of-Flight Mass Spectrometer. *Anal. Chem.* **2009**, *81*, 1792−1800.
(33) Pratt, K. A.; DeMott, P. J.; French, J. R.; Wang, Z.; Westphal, D. L.; Heymsfield, A. J.; Twohy, C. H.; Prenni, A. J.; Prather, K. A. In Situ Detection of Biological Particles in Cloud Ice-Crystals. *Nature Geosci.* **2009**, *2*, 397−400.
(34) Baustian, K. J.; Cziczo, D. J.; Wise, M. E.; Pratt, K. A.; Kulkarni, G.; Hallar, A. G.; Tolbert, M. A. Importance of Aerosol Composition, Mixing State, and Morphology for Heterogeneous Ice Nucleation: A Combined Field and Laboratory Approach. *J. Geophys. Res.: Atmos.* **2012**, *117*, D06217 DOI: 10.1029/2011jd016784.
(35) Zangmeister, C. D.; Pemberton, J. E. Raman Spectroscopy of the Reaction of Sodium Chloride with Nitric Acid: Sodium Nitrate Growth and Effect of Water Exposure. *J. Phys. Chem. A* **2001**, *105*, 3788−3795.
(36) Bones, D. L.; Reid, J. P.; Lienhard, D. M.; Krieger, U. K. Comparing the Mechanism of Water Condensation and Evaporation in Glassy Aerosol. *Proc. Natl. Acad. Sci. U.S.A.* **2012**, *109*, 11613−11618.
(37) Reid, J. P.; Dennis-Smither, B. J.; Kwamena, N. O. A.; Miles, R. E. H.; Hanford, K. L.; Homer, C. J. The Morphology of Aerosol Particles Consisting of Hydrophobic and Hydrophilic Phases: Hydrocarbons, Alcohols and Fatty Acids as the Hydrophobic Component. *Phys. Chem. Chem. Phys.* **2011**, *13*, 15559−15572.
(38) Kwamena, N. O. A.; Buajarern, J.; Reid, J. P. Equilibrium Morphology of Mixed Organic/Inorganic/Aqueous Aerosol Droplets: Investigating the Effect of Relative Humidity and Surfactants. *J. Phys. Chem. A* **2010**, *114*, 5787−5795.